Research Article

Preparation and Photocatalytic Properties of ZnO/CuO/$ZnAl_2O_4$ Composite Hollow Microspheres by One-Pot Method

Yan Jianhui[1, 2], Zhang Li[1, 2]*, Li Xiaoyan[1, 2], Zhang Xiuxiu[1] and Dai Chaohua[1]

[1]School of Chemistry and Chemical Engineering, Hunan Institute of Science and Technology, Yueyang 414006, China
[2]College of Chemistry and Chemical Engineering, Central South University, Changsha 410083, China

Abstract

ZnO/CuO/$ZnAl_2O_4$ composite hollow microspheres have been fabricated using glucose as template by a polyethylene glycol (PEG-4000)-assisted one-pot hydrothermal method. The as-prepared samples were characterized by XRD、SEM 、HRTEM、BET、EDS、UV-Vis DRS and TG-DTA. The photocatalytic activity of the as-prepared samples was evaluated by photocatalytic decolorization of methyl orange (MO) aqueous solution under the irradiation of the simulated sunlight (100 mW/cm^2). The effects of the calcination temperature, amount of PEG and the molar ratio of metal ion on the structure, composition, and photocatalytic properties of the as-prepared samples were investigated in detail. The results indicated that the highest photocatalytic degradation effiency was observed at n(Zn^{2+}):n(Cu^{2+}) ratio of 1:1, 10wt.% mass ratio of PEG to ZnO/CuO/$ZnAl_2O_4$ and calcinations temperature of 600 ◦C. The maximum photocatalytic decoloration rate of 92.4% within 60 min was obtained at 0.5 g·L^{-1} concentration of ZnO/CuO/$ZnAl_2O_4$ photocatalys.

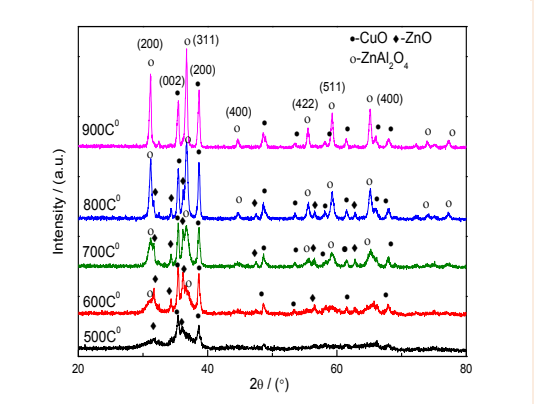

Keywords: hydrothermal method; composite hollow; ZnO/CuO/$ZnAl_2O_4$; microspheres; photocatalytic decoloration; methyl orange

***Correspondence**
Zhang Li,
Email: hgx.zl@163.com

Introduction

Spinel $ZnAl_2O_4$ has been attracting considerable attention since it can be used as catalyst[1], catalyst support[2], and even as optical material[3] due to its high thermal stability, low surface acidity, and high mechanical resistance[4]. However, a broad bandgap of 3.8 eV is the major limitation in achieving high photocatalytic efficiency. To solve the above issue, different methods have been explored and designed in extending light response range and promoting the separation of photoinduced charge carriers, such as improving preparation method[5], doping of noble metal nanoparticles [6] and composite of different semiconductors[7]. In particularly, the coupling of the bandgap structure of both ZnO and $ZnAl_2O_4$ phase in the ZnO/$ZnAl_2O_4$ nanocomposite ensured the efficient separation of photogenerated e- and h^+ pairs, which was prerequisite for the enhanced photocatalytic performance[8,9]. However, conventional powdered photocatalysts have a serious limitation to post-treatment separation in a slurry system after photocatalytic reaction. Furthermore, CuO with a band gap of 1.8 eV have been proven to be beneficial to the catalytic activity enhancement by selecting other semiconductor combined with it[10]. In this study, novel ZnO/CuO/ZnAl2O4 composite hollow microspheres were fabricated by one-pot hydrothermal method.

The structure, composition, morphology, textural, UV–vis absorbing properties of the resulting composites were investigated by SEM, XRD, BET and UV-vis spectra. Subsequently, the photocatalytic activities of the ZnO/CuO/$ZnAl_2O_4$ composites were evaluated by the decolorization of MO.

Experimental

Sample preparation

$ZnO/CuO/ZnAl_2O_4$ sample was prepared by a polyethylene glycol (PEG)-assisted hydrothermal synthetic method using the glucose based carbonaceous materials as template. In a typical synthetic procedure, a mixture of glucose (15 g, as a template agent), $Cu(NO_3)_2 \cdot 3H_2O$ (1.208g), $Al(NO_3)_3 \cdot 9H_2O$ (3.75g) and a certain amount of $Zn(NO_3)_2 \cdot 6H_2O$ was dissolved in deionized water (120 mL), and polyethylene glycol (PEG, as a dispersion agent, ensuring that the content of PEG in catalysts was 5 wt.%, 10 wt.%, 15 wt.%, respectively) was subsequently added with constant stirring to the above solution until complete dissolution. Then ammonia solution ($NH_3 \cdot H_2O$) was added dropwise into the mixture solution under magnetic stirring until the pH reached 7.0. After mixing, the reaction solution was transferred into a 200 mL Teflon-lined autoclave. The autoclave was sealed and kept at 180 ◦C for 24 h, and then cooled to room temperature naturally. After filtration and washing with distilled water and ethanol for several times, the obtained sample was dried in oven at 80 ◦C overnight. Finally, the samples were obtained after annealing under certain temperatures. These samples were denoted as R_1, R_2, R_3, R_4, where R – the ratio of Zn and Cu, and corresponding with Zn/Cu molar ratio of 0, 0.5, 1.0, 1.5, respectively.

Characterization

The crystalline phase and the crystal size of the samples were identified by X-Ray diffraction (XRD, Bruker D8) using Cu Ka radiation (=1.5418A˚) at a scan speed of 0.05◦ s^{-1}, a voltage of 40 kV and a current of 300 mA. The surface morphologies of the samples were observed by scanning electron microscope (SEM, Nova Nano230) operated at 30 kV. The transmission electron microscopy (TEM) measurements were conducted on a Tecnai G2 F20 S-TWIN microscope working at 200 kV. UV–vis diffused reflectance spectra of the samples were obtained using a UV-vis spectrophotometer (UV- 2550, Shimadzu, Japan). $BaSO_4$ was used as a reflectance standard in a UV-vis diffuse reflectance experiment. The chemical composition was analyzed by Energy-dispersive X-ray spectroscopy (EDS) during TEM experiments.

Measurement of photocatalytic activity

The photocatalytic reaction was carried out in homemade tubeshaped quartz reactor including three layers connected with gas collecting devices, and water was used as the external circulation cooling and wind as the internal cooling. The reaction temperature was kept at 25 ± 0.2 ◦C by controlling the external circulation water in the water jacket of the reactor during the entire experiment. The photocatalyst powder (0.3 g) was dispersed by a magnetic stirrer in a 600 mL MO solution with the concentration of 25 $mg \cdot L^{-1}$. A 150-W xenon lamp with λ= 200-900 nm was used as the simulated sunlight source. The luminous intensity was measured at 100 mW/m^2 by the auto-range ST-85 optical radiometer (Photoelectric Instrument Factory of Beijing Normal University). Prior to light illumination, the suspension was strongly magnetically stirred for 30 min in the dark for adsorption/desorption equilibrium. During irradiation, the catalyst was kept in suspension state by a magnetic stirrer. Samples for analysis was extracted through pipette every 10 min and centrifuged immediately. Absorbance of the suspension and initial solution was determined, respectively. A 752 UV-vis spectrophotometer was used at the maximum absorption wavelength (max = 465 nm) of MO. Decoloration rate are presented as C/C_0, where C_0 and C are the initial concentration of MO under adsorption equilibrium and the concentration of MO at different irradiation time, respectively. Experiments for comparison were carried out under the same condition, but one was done without catalyst and another was in the dark. Each set of photocatalytic measurements was repeated three times, and the experimental error was found to be within ±5%.

Results and discussion

XRD study

Figure 1 shows XRD patterns of the samples with addition of 10 wt.% PEG and the starting Zn to Cu molar ratio of 1:1 (R_3) annealed at different temperatures. From Figure 1, the sharp diffraction peaks indicate the poor crystallinity

of the synthesized sample at 500◦C. While most diffraction peaks from this pattern can be indexed to reflections of CuO(JCPDS Card No. 45-0937) and ZnO (JCPDScard, No. 36-1451) except for a minor peak ascribed to a amount of $ZnAl_2O_4$ at 600◦C, indicating that the sample consists of CuO, ZnO and $ZnAl_2O_4$ ternary complexes[11]. With further increasing the calcination temperature, the peaks of ZnO start to decrease in intensity and more $ZnAl_2O_4$ is formed. This indicates that a solid-state reaction of ZnO and Al_2O_3 starts after 600◦C, resulting in the formation of spinel ZnA_2O_4[12]. While calcination temperature increases to 900◦C, the diffraction peaks are mainly indexed to CuO and $ZnAl_2O_4$. It is obvious that five main diffraction peaks of the (200), (311), (422), (511) and (400) reflections are observed in Figure 1, which can be indexed to spinel ZnA_2O_4 (JCPDSCard No. 05-0669). No peaks of ZnO are appeared in the patterns, suggesting that most of ZnO is transferred to ZnA_2O_4.

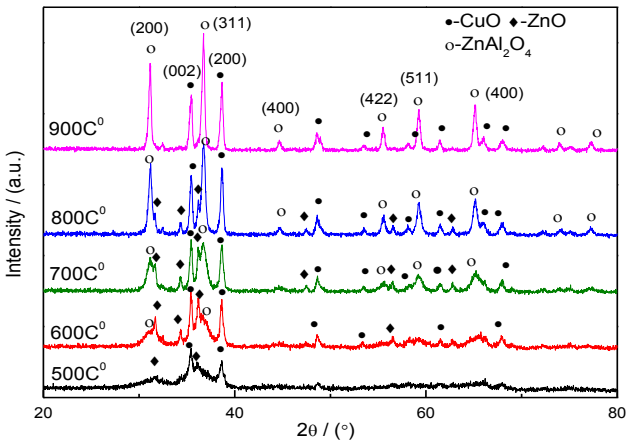

Figure 1 XRD patterns of R_3 samples annealed at different temperatures

Figure 2 shows XRD patterns of the samples with addition of 10 wt.% PEG and different molar ratio of Zn to Cu (R_1、R_2、R_3、R_4) annealed at 600 ◦C. From Figure 2, the XRD patterns of sample with Zn^{2+}/Cu^{2+} ratio of 0:1(R_1) only display a feature of CuO reflections. The intensities of diffraction peaks of ZnO and ZnA_2O_4 oxides gradually increase with the increasing Zn^{2+}/Cu^{2+} ratio, the intensities of diffraction peaks of the sample with Zn^{2+}/Cu^{2+} ratio of 1:1(R_3) are stronger than that of the other samples. It can be speculated that the photocatalytic activity of the sample with Zn^{2+}/Cu^{2+} ratio of 1:1 is the best among the four samples. At this time, the diffraction peaks of CuO exist, indicating that the sample consists of CuO, ZnO and $ZnAl_2O_4$ ternary complexes.

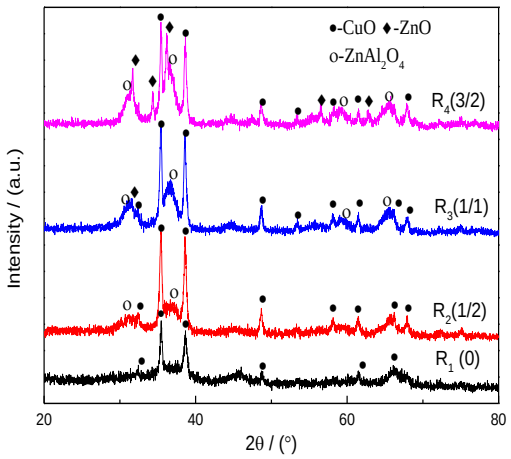

Figure 2 XRD patterns of samples with different Zn/Cu molar ratio

Figure 3 shows XRD patterns of the R_3 samples with different content of PEG annealed at 600 ◦C. It is obvious that the main diffraction peaks (2θ = 35.6, 38.8) can be indexed to the hexagonal phase of CuO (JCPDS Card No. 45-0937), with the increase of PEG additives, the diffraction peak intensity of CuO increases gradually, While the other diffraction peak have no obvious changes, which indicates that adding PEG can slow the reaction process of CuO and Al_2O_3 form $CuAl_2O_4$, so as to to maintain high photocatalytic activity[13].

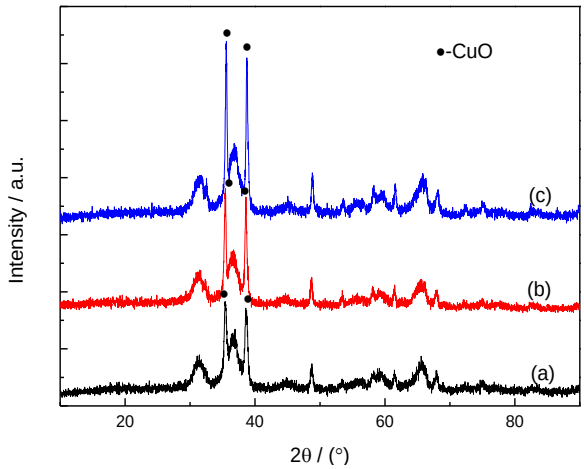

Figure 3 XRD patterns of R_3 samples with different addition of PEG
(a) 5%; (b) 10%; (c) 15%

The morphology analyze

The morphology of the samples with addition of 10 wt.% PEG and the starting Zn to Cu molar ratio of 1:1 (R_3) annealed at 600 ◦C was investigated by SEM in Figure 4. Figure 4a,b show that the samples are nearly in spherical shape with diameters of ca.2-3 μm in the present of glucose, and especially some microspheres are open and hollow due to the removal of carbon by calcinations[14]. This indicates that glucose plays a critical role for the formation of the hollow microspheres, some of which are not flat with rough superstructure[15].

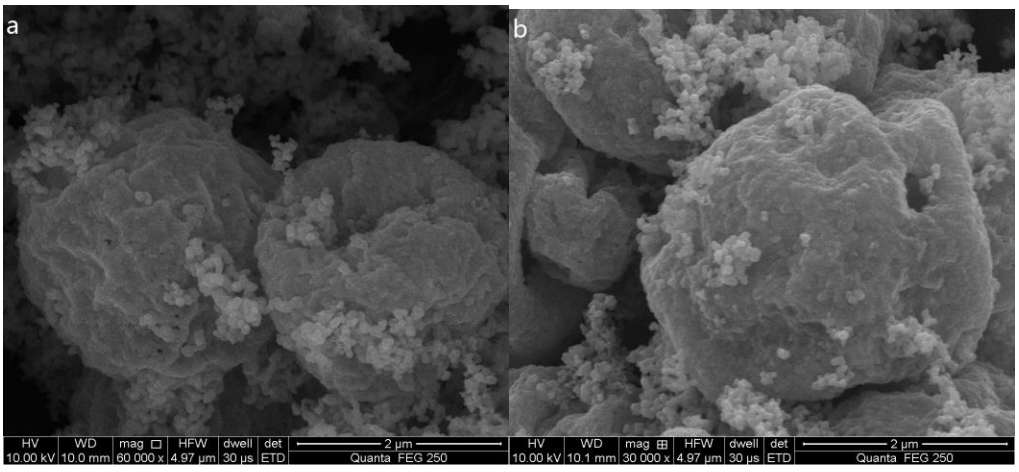

Figure 4 SEM images of R_3 sample

Figure 5 shows the TEM and HRTEM images of the samples with addition of 10 wt.% PEG and the starting Zn to Cu molar ratio of 1:1 (R_3) annealed at 600 ◦C. Fig 5(a) shows that the sample is irregularly spherical and its particle sizes

are relatively identical. The particle size of sample is 15-20 nm. More detailed morphology about the ZnO/CuO/$ZnAl_2O_4$ nanocomposites was indicated by HRTEM (Figure 5(b)). HRTEM image reveals that both ZnO, CuO and $ZnAl_2O_4$ form a heterojunction nanostructure proven by well-defined lattice fringes: the spacing of 2.64 Å represents the lattice-resolved (002) crystalline plane of ZnO phase, the spacing of 2.37 Å represents the lattice-resolved (200) crystalline plane of CuO phase, and the spacing values of 2.86 Å correspond to the (220) facets of $ZnAl_2O_4$ phase, respectively, which are in good agreement with report in Ref. [16].

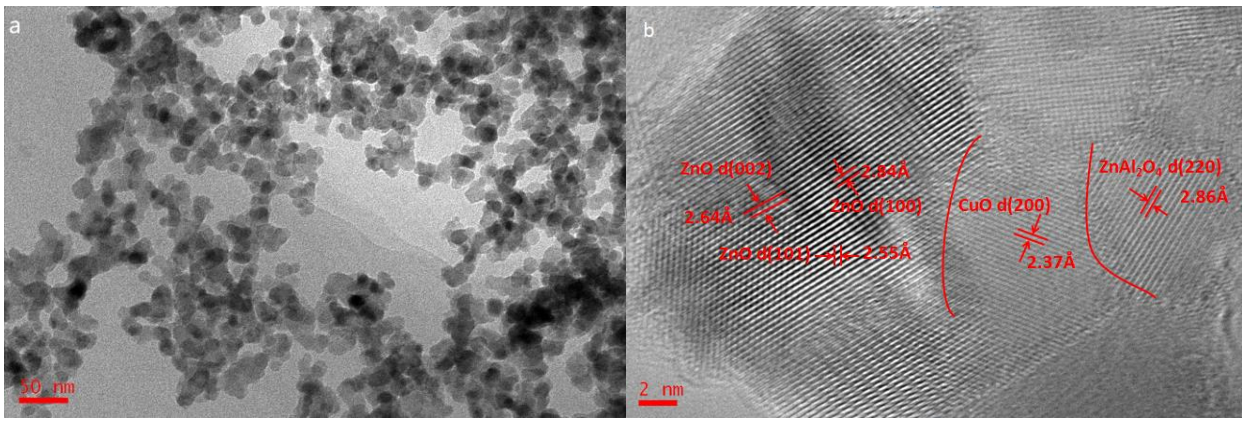

Figure 5 HRTEM images of R_3 sample

The elemental composition of the ZnO/CuO/$ZnAl_2O_4$ sample was further determined by EDS. The EDS survey spectrum (Figure 6a, b) indicates that the prepared sample consists of Zn, Cu, O, Al and C elements. Thus, both XRD and EDS analysis indicate that the as-prepared hollow microspheres are composed of ZnO, CuO and $ZnAl_2O_4$.

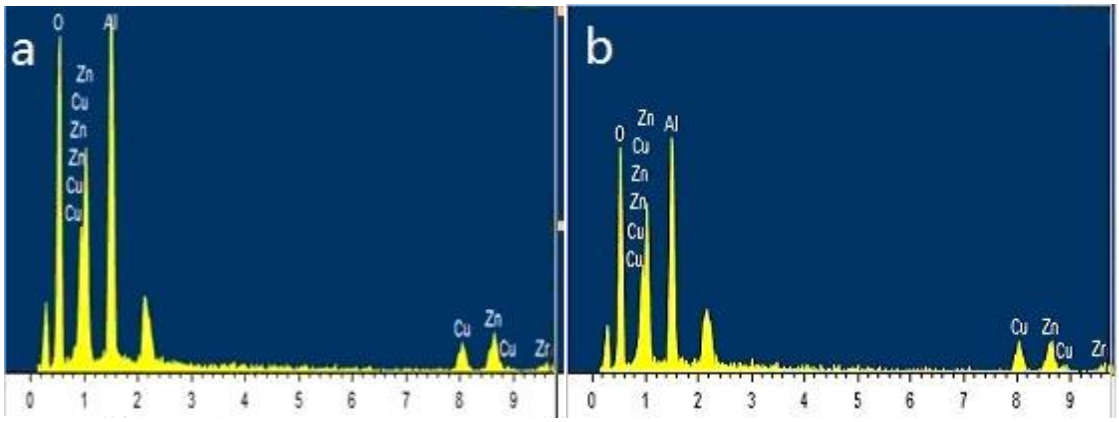

Figure 6 EDS images of R_3 sample

TG-DTA analyze

Fig 7 shows the TG-DTA curves of R_3 sample with addition of 10 wt.% PEG. The first mass loss before 200 °C may be attributed to the evaporation of absorbed water, meanwhile the corresponding endothermic peak is observed from the thermogravimetric curve. The second mass loss occurs at 180-340 °C, and the corresponding exothermic peak at about 280 °C can be ascribed to the decomposition of the residual organic compounds. The third mass loss at 340-600 °C is due to the decomposition of the nitrate and synthesis of the ZnO, CuO and $ZnAl_2O_4$ compounds, and then the mass loss becomes almost constant when the temperature is more than 600 °C. The corresponding endothermic peak at about 720 °C is perhaps owing to the forming of $ZnAl_2O_4$.

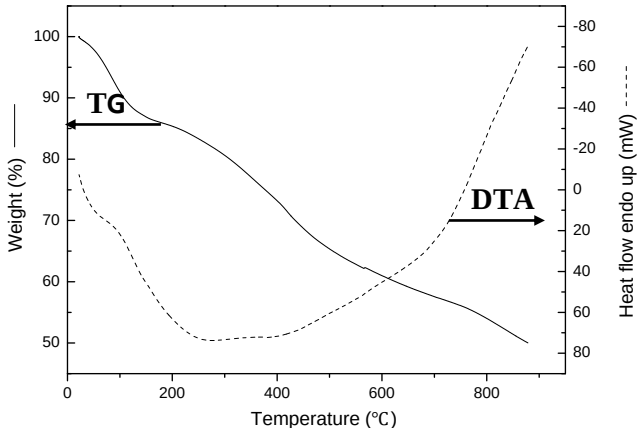

Figure 7 TG/DTA curve for precursor R_3 sample

BET surface area

Table 1 shows the BET surface area, pore volume, and average pore size of samples prepared with addition of 10 wt.% PEG and different molar ratio of Zn to Cu (R_1、R_2、R_3、R_4) annealed at 600 ◦C. The pore volume of as-prepared samples increases gradually in corresponding with average pore size with increasing the molar ratio of Zn/Cu to 1:1, at this point, the pore volume and the average pore size reach the maximum. With increasing the molar ratio of Zn to Cu, the BET surface area increases and reaches its highest value of 229.3 $m^2 \cdot g^{-1}$ with Zn to Cu molar ratio of 3:2. However, when the molar ratio of Zn to Cu is further decreased to 1:1, the surface area of sample decreases from 229.30 to 209.07 $m^2 \cdot g^{-1}$. Consequently, specific surface area of the obtained $ZnO/CuO/ZnAl_2O_4$ has proved to be strongly dependent on the composition. Such phenomena are closely related with the structural feature of different $ZnO/CuO/ZnAl_2O_4$ composites. Moreover, the large porous structure is believed to facilitate the transportation of reactant molecules and products through the interior space due to the interconnected porous networks and to favor the harvesting of exciting light due to enlarged surface area and multiple scattering within the porous framework[17,18].

Table 1 The specific surface property of different n(Zn):n(Cu) ratio samples

Sample	$S_{BET}/(m^2 \cdot g^{-1})$	Adsorption average pore width/nm	Pore volume $(cm^3 \cdot g^{-1})$
R_1 (0)	197.82	8.8	0.56
R_2(1:2)	229.30	10.0	0.72
R_3(1:1)	209.07	11.3	0.73
R_4(3:2)	138.73	10.4	0.45

Figure 8 shows the N_2 adsorption-desorption isotherm and the corresponding pore-size distribution curve for the samples prepared with addition of 10 wt.% PEG and different molar ratio of Zn to Cu (R_1、R_2、R_3、R_4) annealed at 600 ◦C. Figure 8a shows that all the samples have a type IV isotherm according to Brunauer-Deming-Deming-Teller (BDDT) classification with two capillary condensation steps, implying bimodal pore size distributions in the mesoporous (2-50 nm) and macroporous (>50 nm) regions[9,19]. With increasing the molar ratio of Zn to Cu, the

shapes of nitrogen adsorption and desorption isotherms underwent obvious changes, implying a significant variation of pore structures. Firstly, the isotherms corresponding to the R_3 samples show higher absorption at high relative pressures (P/P_0 approaching 1), indicating the formation of larger inter-aggregated pore between the secondary aggregated particles[9,20] and/or an increasing pore volume of interaggregated pores, as further confirmed in Figure 8b. This may be related to the hollowing of the interior space of $ZnO/CuO/ZnAl_2O_4$ microspheres (as shown in Figure 4a and 4b). For the R_3 sample, the bimodal poresize distribution consisting of fine intra-aggregated pores and larger inter-aggregated pores. These mesopores and macropores presumably arise from the interstices among the different-sized nanoparticles within the shells of $ZnO/ZnAl_2O_4$ hollow microspheres. When the molar ratio of Zn to Cu was further increased to 3:2, the hysteresis loop shifted to relative lower pressure (P/P_0) region ($0.65 < P/P_0 < 0.9$), implying the formation of finer intra-aggregated pore within the primary agglomerated particles, as confirmed by a drastic decrease in the corresponding pore volume (Figure 8b).

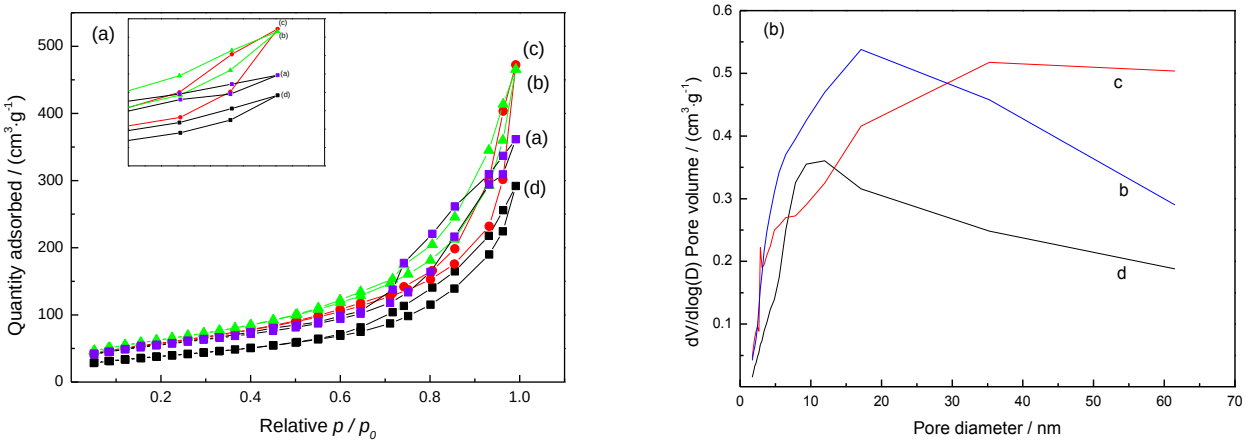

Figure 8 (a) N_2 adsorption-desorption isotherms and (b) pore size distribution curves of different n(Zn):n(Cu) ratio samples (a) R_1 (0); (b) R_2 (1:2); (c) R_3 (1:1); (d) R_4 (3:2)

UV–vis diffuse reflectance spectra

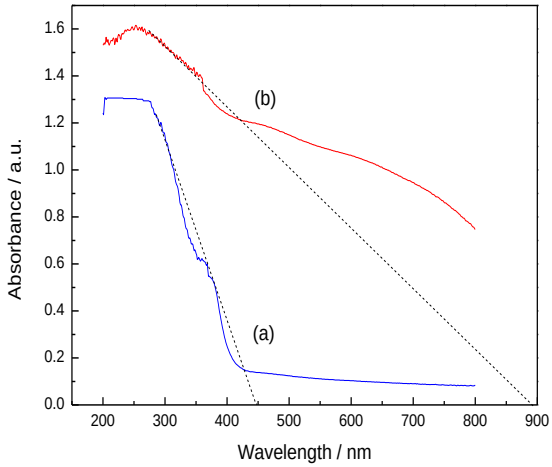

Figure 9 UV-Vis DRS spectra of $ZnO/ZnAl_2O_4$ and R_3 samples (a) $ZnO/ZnAl_2O_4$; (b) R_3

The UV–vis diffuse reflectance spectra (Figure 9) of the samples with addition of 10 wt.% PEG and the starting Zn to Cu molar ratio of 1:1 (R_3) annealed at 600 ◦C. The R_3 sample displays a significant increase in the absorption at

wavelength ≥ 400 nm compared with $ZnO/ZnAl_2O_4$ (Figure 9b). Furthermore, it can be seen that R_3 sample shows a certain absorption in the visible light region (the wavelength ranging from 400 to 800 nm), while no absorption can be observed for $ZnO/ZnAl_2O_4$. This experimental result can be attributed to the coupling interaction between the ZnO, CuO and $ZnAl_2O_4$ phase, the optimizing molar ratio of Zn to Cu and the form of heterojunction structure, which leads to the enhancement of utilization of light and photocatalytic activity[21].

Photocatalytic activity

Effect of calcination temperature on photocatalytic degradation activity:

Figure 10 reveals the photocatalytic activities of the $ZnO/CuO/ZnAl_2O_4$ nanocomposites with addition of 10 wt.% PEG and the starting Zn to Cu molar ratio of 1:1 annealed at different temperatures. From Figure 10, the photocatalytic activities vary greatly for the samples. The sample annealed at 600 °C shows the highest photocatalytic activity. The maximum photocatalytic degradation rate of 92.4% in 60 min is obtained. For the other samples annealed at 500, 700, 800, and 900 °C, the degradation rates of MO within 60 min are decreased. The difference in photocatalytic activity may be ascribed to the crystalline quality of the nanocomposition. The sample annealed at 500 °C shows the lower activity than that annealed at 600 °C, which may be ascribed to the relatively poor crystallinity(shown in Figure 1). The sample annealed at 600 °C shows a better crystalline quality. The photocatalyst with good crystallization can provide a shorter migration distance for electrons and holes and reduce the chances of their recombination. Therefore, the photocatalytic reaction efficiency is accelerated and the catalytic activity is improved [22].

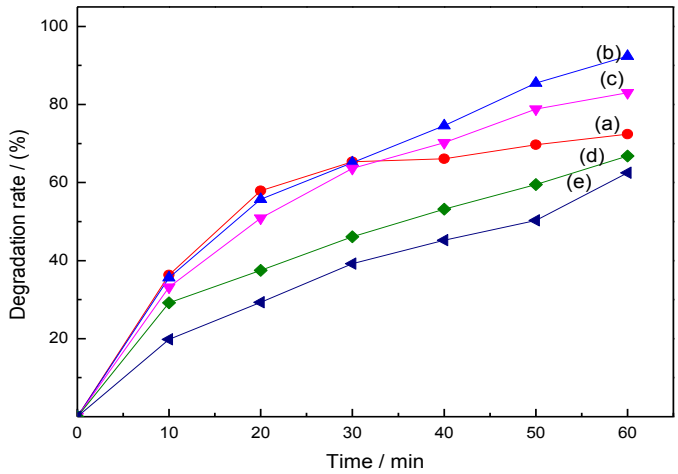

Figure 10 Effects of calcination temperature on photocatalytic activity
(a) 500℃; (b) 600℃; (c) 700℃; (d) 800℃; (e) 900℃

Effect of the molar ratio of Zn to Cu on photocatalytic degradation activity:

Figure 11 reveals the photocatalytic activities of the $ZnO/CuO/ZnAl_2O_4$ nanocomposites with addition of 10 wt.% PEG and different molar ratio of Zn to Cu (R_1、R_2、R_3、R_4) annealed at 600 ◦C. It can be seen that the photocatalytic activities of $ZnO/CuO/ZnAl_2O_4$ samples first increase with the molar ratio of Zn to Cu up to 1:1, and then slightly decrease when the molar ratio exceeds 1:1. The sample with the starting Zn to Cu molar ratio of 1:1 shows the highest photocatalytic activity. The maximum photocatalytic degradation rate of 92.4% in 60 min is obtained. For the other samples with the starting Zn to Cu molar ratio of 1:2, 3:2, the degradation rates of MO within 60 min are all decreased. The difference in photocatalytic activity may be ascribed to the BET surface area and the the nanocomposition[23,24]. Although the sample with the starting Zn to Cu molar ratio of 1:2 possesses a larger specific surface area, the photocatalytic activity is lower. The reason is attributed to the existing of heterojuction and the content of ZnO, CuO in the $ZnO/CuO/ZnAl_2O_4$ nanocomposite. When they are coupled together to form a

heterostructure which is energetically favorable to separat photogenerated e− and h+ pairs. The efficient separation of the photogenerated e− and h+ pairs is regarded as the key factor for the high photocatalytic activities. On the other hand, the high photocatalytic activity of sample with the Zn to Cu molar ratio of 1:1 is also attributed to the higher specific surface area than the sample with the starting Zn to Cu molar ratio of 3:2 (shown in Table 1). A larger surface area provides more surface active sites for the adsorption of reactants molecules, making the photocatalytic process more efficient [25].

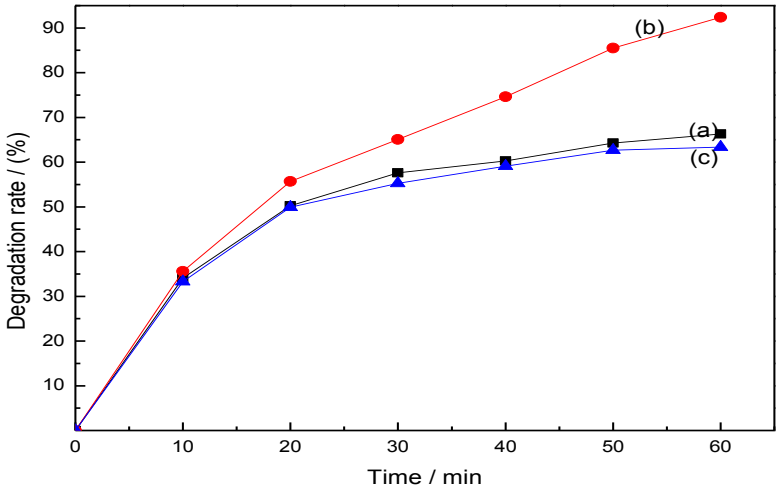

Figure 11 Effects of different Zn/Cu molar ratio on photocatalytic activity
(a) Zn/Cu=1:2; (b) Zn/Cu =1:1; (c) Zn/Cu=3:2

Conclusions

1. The ZnO/CuO/$ZnAl_2O_4$ composite hollow microspheres have been fabricated using glucose as template by a polyethylene glycol (PEG)-assisted one-pot hydrothermal method and characterized in detail. The results showed that the coupling of the ZnO, CuO and $ZnAl_2O_4$ not only enhanced light absorption range compared with ZnO/$ZnAl_2O_4$ but increased BET.
2. The photocatalytic degradation activity of the ZnO/CuO/$ZnAl_2O_4$ nanocomposites can be improved by varying the molar ratio of Zn to Cu and calination temperature.
3. The decoloration rate of 92.4% for MO in 60 min is obtained at the molar ratio of Zn to Cu of 1:1, PEG of 10 wt.% and annealing temperature of 600 °C, which may be attributed to the fact that ZnO, CuO and $ZnAl_2O_4$ can form heterojunction structure.

Acknowledgements

This project was financially supported by the National Nature Science Foundation of China (No. 21271071, 21306041), and Aid Program for Science and Technology Innovative Research Team in Higher Educational Institutions of Hunan Province（No.12K117）.

References

[1] S. Farhadi, S. Panahandehjoo, Spinel-type zinc aluminate ($ZnAl_2O_4$) nanoparticles prepared by the co-precipitation method: a novel, green and recyclable heterogeneous catalyst for the acetylation of amines, alcohols and phenols under solvent-free conditions, Applied Catalysis A: General 382 (2010) 293–302.
[2] A. D. Ballarini, S. A. Bocanegra, A. A. Castro, S. R. de Miguel, O. A. Scelza, Characterization of $ZnAl_2O_4$ obtained by different methods and used as catalytic support of Pt, Catalysis Letters 129 (2009) 293–302.

[3] Y. Wang, K. Wu, As a whole: crystalline zinc aluminate nanotube array-nanonet, Journal of the American Chemical Society 127 (2005) 9686–9687.
[4] M. Zawadzzki, Synthesis of nanosized and microporous zinc aluminate spinel by microwave assisted hydrothermal method (microwave-hydrothermal synthesis of $ZnAl_2O_4$), Solid State Sciences 8 (2006) 14–18.
[5] F. Conrad, C. Massue, S. Kuhl, E. Kunkes, F. Girgsdies, I. Kasatkin, B. Zhang, M. Friedrich, Y. Luo, M. Armbruster, G. R. Patzke, M. Behrens. Microwave hydrothermal synthesis and characterization of nanostructured copper substituted ZnM_2O_4 (M = Al, Ga) spinels as precursors for thermally stable Cu catalysts, Nanoscale 4 (2012) 2018–2028.
[6] Z. Zhu, Q. Zhao, X. Li, et al, Photocatalytic performances and activities in Ag-doped $ZnAl_2O_4$ nanorods studied by FTIR spectroscopy, Catalysis Science & Technology 3(2013) 788-796.
[7] L. Kong, X. Yin, F. Ye, et al, Electromagnetic wave absorption properties of ZnO-based materials modified with $ZnAl_2O_4$ nanograins, The Journal of Physical Chemistry C 117(2013) 2135-2146.
[8] X. F. Zhao, L. Wang, X. Xu, X. D. Lei, S. L. Xu, F. Z, Zhang, Fabrication and photocatalytic properties of novel ZnO/$ZnAl_2O_4$ nanocomposite with $ZnAl_2O_4$ dispersed inside ZnO network, AIChE Journal 58 (2012) 573–582.
[9] L. Zhang, J.H. Yan, M. J. Zhou, Fabrication and photocatalytic properties of spheres-in-spheres ZnO/$ZnAl_2O_4$ composite hollow microspheres, Applied Surface Science 268 (2013) 237– 245
[10] J. H. Yan, M. H. Yao, L. Zhang, Y. G. Tang, H. H. Yang, Photocatalytic H_2 evolution activity of CuO/ZrO_2 composite catalyst under simulated sunlight irradiation, Journal of Central South University of Technology 18 (2011) 56–62.
[11] X. L. Duan, D. R. Yuan, X. Q. Wang, et al, Synthesis and characterization of nanocrystalline zinc aluminum spinel by a new sol-gel method, J. Sol-gel Sci. technol. 35(2005)221-224.
[12] D. Carriazo, M. del Arco, E. Garcia-Lopez, G. Marci, C. Martin, L. Palmisano, V. Rives, Zn, Al hydrotalcites calcined at different temperatures: Preparation, characterization and photocatalytic activity in gas-solid regime, Journal of Molecular Catalysis A: Chemical 342–343(2011)83-90
[13] L. ZHANG, Y.N. Liu , Y. Liu, J.H. Yan，Effects of PEG on synthesis and photocatalytic property of CuO/Al_2O_3 photocatalysts, Transactions of Nonferrous Metals Society of China (In Chinese) 24(2014) 204-210
[14] C. L.Yu, W. Q. Zhou, K. Yang, Hydrothermal synthesis of hemisphere-like F-doped anatase TiO_2 with visible light photocatalytic activity, J. Mater. Sci. 45(2010) 5756-5761.
[15] X. Wu, G. Q. Lu, L. Z. Wang, Shell-in-shell TiO_2 hollow spheres synthesized by one-pot hydrothermal method for dye-sensitized solar cell application, Energy Environ. Sci. 4(2011) 3565-3572.
[16] L. Zhang, J.H. Yan, M.J. Zhou, Yan-ping Yu, Ye Liu, You-nian Liu, Photocatalytic degradation and inactivation of *Escherichia coli* by ZnO/$ZnAl_2O_4$ with heteronanostructures, Transactions of Nonferrous Metals Society of China 24(2014) 743-749
[17] J. Yu, J.C. Yu, M.K.P. Leung, W. Ho, B. Cheng, X. Zhao, J. Zhao, Effects of acidic and basic hydrolysis catalysts on the photocatalytic activity and microstructures of bimodal mesoporous titania, Journal of Catalysis 217 (2003) 69–78.
[18] X.C. Wang, J.C. Yu, Y.L. Chen, L. Wu, X.Z. Fu, ZrO2-modified mesoporous nanocrystalline TiO2-xNx as efficient visible light photocatalysts, Environmental Science and Technology 40 (2006) 2369–2374.
[19] B. Yin, J. T. Wang, W. Xu, et al, Preparation of TiO_2/mesoporous carbon composites and their photocatalytic performance for methyl orange degradation, New Carbon Materials 28 (2013) 47-54.
[20] L. Zhang, J. H. Yan, M. J. Zhou, et al, Preparation and photocatalytic property of hollow sphere-like ZnO/$ZnAl_2O_4$ composite photocatalysts with high specific surface area. Journal of Inorganic Chemistry (In Chinese) 28(2012) 1827-1834.
[21] S. S. Lee, H. W. Bai, Z. Y. Liu, et al, Optimization and an insightful properties-activity study of electrospun TiO_2/CuO composite nanofibers for efficient photocatalytic H_2 generation, Appl. Catal. B: Environ. 140-141(2013) 68-81.
[22] D. LI, H. HANEDA, Morphologies of zinc oxide particles and their effects on photocatalysis. Chemosphere 51(2003)129−137.

[23] H. J. Zhang, G. H. Chen, D. W. Bahnemann, Photoelectrocatalytic materials for environmental applications, J. Mater. Chem. 19(2009) 5089-5121.
[24] J. Zhang, Q. Xu, Z. C. Feng, et al, Importance of the relationship between surface phases and photocatalytic activity of TiO_2, Angew. Chem. Int Ed. 47(2008) 1766-1769.
[25] F. B. Li, X. Z. Li, M. F. Hou, K. W. Cheah, W. C. H. Choy. Enhanced photo-catalytic activity of Ce^{3+}-TiO_2 for 2-mercaptobenzothiazole degradation in aqueous suspension for odour control, Appl Catal Gen 285(2005)181−189.

Publication History
Received 29th Oct 2014
Revised 15th Nov 2014
Accepted 22nd Nov 2014
Online 30th Nov 2014